NASA Technical Memorandum 100205
ICOMP-87-7

Similar Solutions for Viscous Hypersonic Flow Over a Slender Three-Fourths-Power Body of Resolution

Chin-Shun Lin
Institute for Computational Mechanics in Propulsion
Lewis Research Center
Cleveland, Ohio

December 1987

NASA

SIMILAR SOLUTIONS FOR VISCOUS HYPERSONIC FLOW OVER A SLENDER THREE-FOURTHS-POWER BODY OF REVOLUTION

C.S. Lin
National Aeronautics and Space Administration
Lewis Research Center
Cleveland, Ohio 44135

E-3803

SUMMARY

For hypersonic flow with a shock wave, there is a similar solution consistent throughout the viscous and inviscid layers along a very slender three-fourths-power body of revolution. The strong pressure interaction problem can then be treated by the method of similarity. In the present study, numerical calculations are performed in the viscous region with the edge pressure distribution known from the inviscid similar solutions. The compressible laminar boundary-layer equations are transformed into a system of ordinary differential equations. The resulting two-point boundary value problem is then solved by the Runge-Kutta method with a modified Newton's method for the corresponding boundary conditions. The effects of wall temperature, mass bleeding, and body transverse curvature are investigated. The induced pressure, displacement thickness, skin friction, and heat transfer due to the previously mentioned parameters are estimated and analyzed.

INTRODUCTION

At hypersonic speeds, flow is decelerated by the work of compression and viscous dissipation, therefore a high-temperature gas is produced in the boundary layer. The density of the hot gas is very low, so the mass flux in this boundary layer is small. Because of this high temperature, the thickness of the boundary layer on the body surface increases and the streamlines in the flow external to the boundary layer are displaced outward. The displacement thickness may be comparable to or may even exceed the body thickness, so that the effect of body transverse curvature is significant. The effective thickening of the body can also induce a large pressure, which is transmitted into the external inviscid field along the Mach lines. These pressures are then transmitted essentially without change through the boundary layer and, in turn, govern the growth of the boundary layer. Along with the pressure interaction, the vorticity interaction may also occur because of the curved shock wave. Thus, the boundary-layer structure will be governed not only by the pressure gradient, but also by the vorticity at the edge of the boundary layer (ref. 1).

Another important fact is that high temperature can also cause the gas to depart from the perfect-gas behavior. Thus the high-temperature gasdynamics needs to be taken into account. The viscous-inviscid interaction and the physical-chemical phenomena are more or less dependent on each other - a fact that makes the theoretical investigation much more difficult. In the present study, we assume that the perfect-gas relation holds and that the vorticity interaction is negligible (i.e., only the pressure interaction is considered).

For hypersonic flow with a shock wave, a similar solution is found to be consistent throughout the viscous and inviscid layers along a very slender

three-fourths-power body of revolution. The strong pressure interaction problem can then be treated by the method of similarity. In the present study, numerical calculations are performed in the viscous region with the edge pressure distribution known from the inviscid similar solutions. The compressible laminar boundary-layer equations are transformed into a set of ordinary differential equations, and a two-point boundary value problem results. The Runge-Kutta method is then used with a modified Newton's method to solve the resulting simultaneous nonlinear equations for the corresponding boundary conditions.

Although the thermodynamic and fluid dynamic phenomena associated with flight at hypersonic speeds have been the subject of intensive research for the past decades, only a few studies of the effects of body transverse curvature and mass bleeding have been carried out (refs. 2 to 7). The purpose of this study is to contribute to the investigation of the effects of wall temperature, mass bleeding, and body transverse curvature on the strong pressure interaction region during hypersonic flights. The induced pressure, displacement thickness, skin friction, and heat transfer are then analyzed based on these parameters.

GOVERNING EQUATIONS AND BOUNDARY CONDITIONS

For axially symmetric flow with body forces neglected, the compressible laminar boundary-layer equations can be written as follows:

Continuity:

$$\frac{\partial}{\partial X}(\rho r U) + \frac{\partial}{\partial Y}(\rho r V) = 0 \tag{1}$$

Momentum:

$$\rho U \frac{\partial U}{\partial X} + \rho V \frac{\partial U}{\partial Y} = \rho_e U_e \frac{\partial U_e}{\partial X} + \frac{1}{r} \frac{\partial}{\partial Y}\left(\mu r \frac{\partial U}{\partial Y}\right) \tag{2}$$

Energy:

$$\rho U \frac{\partial H}{\partial X} + \rho V \frac{\partial H}{\partial Y} = \frac{1}{r} \frac{\partial}{\partial Y} \left(\frac{\mu}{Pr} r \frac{\partial H}{\partial Y}\right) + \frac{1}{r} \frac{\partial}{\partial Y} \left\{\left(1 - \frac{1}{Pr}\right)\mu r \frac{\partial}{\partial Y} \left(\frac{U^2}{2}\right)\right\} \tag{3}$$

where

$$r = r_w + Y \cos \bar{\alpha}_w$$

with $\bar{\alpha}_w \ll 1$. The coordinate system is shown in figure 1. For these equations, U and V are the velocity components in the X and Y directions, respectively, H is the total enthalpy, and the Prandtl number $Pr = C_p\mu/k$, where C_p is the specific heat at constant pressure, μ is the coefficient of molecular viscosity, and k is the coefficient of thermal conductivity. The variables P, ρ, and T are the pressure, density, and temperature, respectively, governed by the perfect-gas law

$$P = \rho \tilde{R} T$$

where $\tilde{R}$ is the gas constant.

The boundary conditions for the flow problem considered here are

$$U(X,0) = 0$$

$$V(X,0) = V_w(X)$$

$$H(X,0) = H_w(X)$$

$$\lim_{Y \to \infty} U(X,Y) = U_e(X)$$

$$\lim_{Y \to \infty} H(X,Y) = H_e(X)$$

TRANSFORMATION

By extending the Mangler-Levy-Lees transformation, we can transform the coordinate axes (X,Y) into (ξ,η) by

$$\xi = \int_0^X \rho_w \mu_w U_e r_w^2 \, dX \quad \text{and} \quad \eta = \frac{U_e}{\sqrt{2\xi}} \int_0^Y \rho r \, dY$$

from which we derive

$$\frac{d\xi}{dX} = \rho_w \mu_w U_e r_w^2 \quad \text{and} \quad \frac{\partial \eta}{\partial Y} = \frac{\rho r U_e}{\sqrt{2\xi}}$$

Further, when the dependent variables F and G are defined by

$$\frac{\partial F}{\partial \eta} = \frac{U}{U_e} \quad \text{and} \quad G = \frac{H}{H_e}$$

the laminar boundary-layer equations become (ref. 2)

$$\rho V r = -\left[\xi_X \left(\sqrt{2\xi} F_\xi + \frac{F}{\sqrt{2\xi}}\right) + \sqrt{2\xi}\, \eta_X F_\eta\right] \tag{4}$$

$$[(NR)F_{\eta\eta}]_\eta + FF_{\eta\eta} + 2\frac{d \ln U_e}{d \ln \xi}\left(\frac{\rho_e}{\rho} - F_\eta^2\right) = 2\xi(F_\eta F_{\xi\eta} - F_\xi F_{\eta\eta}) \tag{5}$$

$$\left[\left(\frac{NR}{Pr}\right)G_\eta\right]_\eta + FG_\eta + \frac{U_e^2}{H_e}\left[\left(1 - \frac{1}{Pr}\right)(NR)F_\eta F_{\eta\eta}\right]_\eta = 2\xi(F_\eta G_\xi - F_\xi G_\eta) \qquad (6)$$

where

$$N = \frac{\rho\mu}{\rho_w\mu_w}$$

and

$$R = \frac{r^2}{r_w^2} \approx 1 + \frac{2\cos\bar{\alpha}_w\sqrt{2\xi}}{\rho_e U_e r_w^2}\int_0^\eta \frac{\rho_e}{\rho}\,d\eta$$

In order to have similar solutions the following similarity criteria are required for an isoenergetic flow outside the boundary layer where H_e is constant (ref. 8):

(1) NR = constant or NR is a function of F and G.

(2) Pr = 1 or U_e^2/H_e = constant when either Pr = constant or Pr is a function of F and G.

(3) $2\frac{d\ln U_e}{d\ln\xi}\left(\frac{\rho_e}{\rho} - F_\eta^2\right)$ = constant or $2\frac{d\ln U_e}{d\ln\xi}\left(\frac{\rho_e}{\rho} - F_\eta^2\right)$ is a function of F and G.

(4) F(0) = constant.

(5) G(0) = constant or $G_\eta(0) = 0$.

There are only three physical situations in which we expect the similarity to hold (ref. 1): (1) The constant-pressure solutions can be obtained if the pressure and the streamwise velocity at the edge of the boundary layer are constant along the boundary. (2) The stagnation-point solutions are obtained by assuming a stagnation point for the inviscid flow and the boundary layer lying on the body within the stagnation region. (3) The third situation is the hypersonic solution which is studied in the present work. In order to satisfy the above similarity criteria for the hypersonic case, we make the following assumptions:

(1) For hypersonic flow, $U_e^2/H_e = 2$.

(2) T_w is constant and $U_e = U_\infty - O\left(1/M_\infty^2\right) = U_\infty$.

(3) Pr = 0.72 and $\gamma = 1.4$.

(4) μ is a power function of T: $\mu/\mu_\infty = (T/T_\infty)^\omega$ where $\omega = 0.75$

(5) $P \propto X^n$ and $r_w \propto X^m$ where $2m + n = 1$.

(6) $V_w \propto X^{-1/4}$.

It is noted that for a three-fourths-power body of revolution $m = \frac{3}{4}$, so we have $n = -\frac{1}{2}$. This condition is consistent with the inviscid hypersonic similarity criterion. The pressure distribution $P \propto X^{-\frac{1}{2}}$ has been confirmed by the experimental work for a flat plate (refs. 9 and 10).

The similarity boundary-layer differential equations are then in the form (ref. 2)

$$[(NR)F_{\eta\eta}]_\eta + FF_{\eta\eta} + \frac{\gamma - 1}{4\gamma}\left(G - F_\eta^2\right) = 0 \tag{7}$$

$$\left[\left(\frac{NR}{Pr}\right)G_\eta\right]_\eta + FG_\eta + 2\left[\left(1 - \frac{1}{Pr}\right)(NR)F_\eta F_{\eta\eta}\right]_\eta = 0 \tag{8}$$

where

$$N = \left(\frac{G - F_\eta^2}{G_w}\right)^{\omega-1}$$

$$R = 1 + A\int_0^\eta \left(G - F_\eta^2\right)d\eta$$

with the transverse curvature effect parameter A given by

$$A = \frac{\gamma - 1}{\gamma}\frac{\cos\bar{\alpha}_w}{\sqrt{\alpha\beta^2}}\sqrt{\frac{\mu_w U_e}{\tilde{R}T_w}} = \text{constant} \tag{9}$$

and the mass bleeding effect parameter F given by

$$F_w = \frac{-V_w X^{\frac{1}{4}}}{\sqrt{(\tilde{R})T_w\mu_w U_e\alpha}} \tag{10}$$

The constants α and β satisfy the relations $P = \alpha X^{-\frac{1}{2}}$ and $r_w = \beta X^{\frac{3}{4}}$, respectively.

COMPUTATIONAL METHOD

To solve equations (7) and (8), we define a set of new dependent variables

$$Y_1 = F$$

$$Y_2 = F'$$

$$Y_3 = F''$$

$$Y_4 = G$$

$$Y_5 = G'$$

Equations (7) and (8) are reduced to a system of first-order ordinary differential equations:

$$Y_1' = Y_2 \tag{11}$$

$$Y_2' = Y_3 \tag{12}$$

$$Y_3' = -\left[\frac{\Phi_1 + (NR)_\eta Y_3}{NR}\right] \tag{13}$$

$$Y_4' = Y_5 \tag{14}$$

$$Y_5' = -\left\{\frac{(NR)_\eta}{Pr} Y_5 + Y_1 Y_5 + 2\left(1 - \frac{1}{Pr}\right)\left[(NR)Y_3^2 - \Phi_1 Y_2\right]\right\} \Big/ \left(\frac{NR}{Pr}\right) \tag{15}$$

where

$$\Phi_1 = Y_1 Y_3 + \frac{\gamma - 1}{4\gamma}\left(Y_4 - Y_2^2\right)$$

$$NR = \left(\frac{Y_4 - Y_2^2}{Y_4(0)}\right)^{\omega-1} (1 + A\Phi_2)$$

$$\Phi_2 = \int_0^\eta \left(Y_4 - Y_2^2\right) d\eta$$

and

$$(NR)_\eta = \left(\frac{Y_4 - Y_2^2}{Y_4(0)}\right)^{\omega-1} A\left(Y_4 - Y_2^2\right) + (\omega - 1)\left(\frac{Y_4 - Y_2^2}{Y_4(0)}\right)^{\omega-2} \left(\frac{Y_5 - 2Y_2 Y_3}{Y_4(0)}\right)(1 + A\Phi_2)$$

The corresponding boundary conditions become

$$\left.\begin{aligned} Y_1 &= F_w \quad \text{(mass bleeding)} \\ Y_2 &= 0 \\ Y_4 &= G_w \quad \text{(constant wall temperature)} \end{aligned}\right\} \quad \text{at } \eta = 0$$

$$\left.\begin{aligned} Y_2 &= 1 \\ Y_4 &= 1 \end{aligned}\right\} \quad \text{as } \eta \to \infty$$

Obviously, it is a two-point boundary value problem.

This two-point boundary value problem can be solved by using the following algorithm:

(1) Set $i = 1$ and guess $Y_3(0)$ and $Y_5(0)$.

(2) Use the Runge-Kutta method to integrate the system of equations (11) to (15).

(3) Check the terminal conditions:

$$e_2^i = Y_2^i(\infty) - 1$$

$$e_4^i = Y_4^i(\infty) - 1$$

If $|e_2^i| < \varepsilon_2$ and $|e_4^i| < \varepsilon_4$, the solutions are obtained. Otherwise, use the modified Newton's method to correct the initial guesses:

$$\begin{bmatrix} Y_3^{i+1}(0) \\ Y_5^{i+1}(0) \end{bmatrix} = \begin{bmatrix} Y_3^i(0) \\ Y_5^i(0) \end{bmatrix} - a\left(\frac{\partial e}{\partial \zeta}\right)_i e^i$$

where

$$e = \begin{bmatrix} e_2 \\ e_4 \end{bmatrix} \qquad \zeta = \begin{bmatrix} Y_3(0) \\ Y_5(0) \end{bmatrix} \qquad 0 < a < 1$$

(4) Set $i = i+1$, then go to step (2).

SOLUTIONS IN STRONG PRESSURE INTERACTION REGION

The outer edge pressure P/P_∞ and the displacement thickness δ^*/X can be expressed as an asymptotic series of the form

$$\frac{P}{P_\infty} = P_0 \bar{x}^{-\frac{1}{2}} \left[1 + \frac{P_1 M_\infty \bar{\alpha}_w}{\bar{x}^{\frac{1}{2}}} + \frac{P_2 + P_3 (M_\infty \bar{\alpha}_w)^2}{\bar{x}} + \cdots\right]$$

$$\frac{\delta^*}{X} = \delta_0 \frac{\bar{x}^{-\frac{1}{2}}}{M_\infty} \left[1 + \frac{\delta_1 M_\infty \bar{\alpha}_w}{\bar{x}^{\frac{1}{2}}} + \frac{\delta_2 + \delta_3 (M_\infty \bar{\alpha}_w)^2}{\bar{x}} + \cdots\right]$$

where δ_m's and P_m's are the constants to be determined, $\bar{x}$ is the pressure interaction parameter defined by

$$\bar{x} = \frac{M_\infty^{2+\omega}}{\sqrt{Re_{x,\infty}}}$$

and $\bar{\alpha}_w$ is the surface inclination angle (fig. 1). With the similar hypersonic inviscid solution (ref. 1),

$$\frac{P}{P_\infty} = \Pi M_\infty^2 \left(\frac{dr_w}{dX} + \frac{d\delta^*}{dX} \right)^2$$

we can, in principle, obtain all the terms P_m's and δ_m's after considerable mathematical manipulations. For simplicity we only consider the zeroth-order solutions; that is, we assume that the interaction parameter $\bar{\chi}$ is very large. We then have the following expressions for P_0 and δ_0 (ref. 11):

$$P_0 = \frac{9}{16} (\Pi) \delta_0^2 \left(1 + \frac{r_w}{\delta^*} \right)^2 \tag{16}$$

$$\delta_0^2 = \frac{(\gamma - 1)\sqrt{2}}{3\sqrt{\Pi}} \kappa \frac{1}{1 + \frac{r_w}{\delta^*}} \tag{17}$$

and the corresponding zeroth-order solutions for a three-fourths-power body of revolution are

$$\frac{P}{P_\infty} = \frac{9}{16} \sqrt{\Pi} \frac{2(\gamma - 1)}{3} \left(1 + \frac{\gamma_w}{\delta^*} \right) \kappa \bar{\chi} \tag{18}$$

$$M_\infty \frac{\delta^*}{X} = \frac{4}{3} \frac{1}{\sqrt{\Pi}} \frac{1}{1 + r_w/\delta^*} \left(\frac{P}{P_\infty} \right)^{1/2} \tag{19}$$

$$C_{f\infty} \sqrt{Re_{X,\infty}} \left(\frac{T_\infty}{T_w} \right)^{\frac{\omega - 1}{2}} = 2 \left(\frac{P}{P_\infty} \right)^{1/2} F''(0) \tag{20}$$

$$\frac{Nu_\infty}{\sqrt{Re_{X,\infty}}} \left(\frac{T_\infty}{T_w} \right)^{\frac{\omega - 1}{2}} = \frac{G'(0)}{h_r/H_e - G(0)} \left(\frac{P}{P_\infty} \right)^{1/2} \tag{21}$$

The value of Π is 1.296 as determined by Yasuhara (ref. 12). The Reynolds number Re, skin friction coefficient C_f, and the Nusselt number Nu are all based on free-stream values and are given by

$$C_{f\infty} = \frac{2}{\rho_\infty U_\infty^2} \left(\mu \frac{\partial U}{\partial Y} \right)_w \tag{22}$$

$$Re_{X,\infty} = \frac{\rho_\infty U_\infty X}{\mu_\infty} \tag{23}$$

$$Nu_\infty = St_\infty Re_{x,\infty} Pr \tag{24}$$

with the Stanton number St given as

$$St_\infty = \frac{\left(k \frac{\partial T}{\partial Y}\right)_w}{\rho_\infty U_\infty (h_r - h_w)} \tag{25}$$

and h_r given as the adiabatic wall enthalpy or recovery enthalpy. Equations (22) and (25) can be reexpressed as the following forms:

$$C_{f\infty} = \frac{2\mu_\infty}{\rho_\infty U_\infty^2} \left(\frac{H_e}{h_\infty}\right)^\omega \left[G(0)\right]^\omega F''(0) \tag{26}$$

$$\frac{St_\infty}{C_{f\infty}} = \frac{G'(0)}{2PrF''(0)\left[h_r/H_e - G(0)\right]} \tag{27}$$

For convenience equations (26) and (27), instead of equations (20) and (21), will be used in our analysis and comparison.

RESULTS AND DISCUSSION

The displacement thickness δ^* for the axisymmetric boundary layer is defined by

$$\int_0^{\delta^*} (\rho_e U_e) 2\pi r \, dY = \int_0^{\delta} (\rho_e U_e - \rho U) 2\pi r \, dY$$

For a hypersonic flow over a slender body of revolution, we can obtain

$$\frac{\delta^*}{r_w} = \sqrt{1 + A\kappa} - 1 \tag{28}$$

where the integral factor κ is defined as

$$\kappa = \int_0^\infty (G - F'^2) d\eta$$

If the effect of the transverse curvature is neglected, we then have

$$\frac{\delta_M^*}{r_w} = \tfrac{1}{2}A\kappa_M \tag{29}$$

where δ_M^* denotes the displacement thickness calculated in Mangler's transformation and κ_M is the value of κ for $A = 0$. Although figure 2 shows that κ decreases as A decreases, the value of δ^*/r_w calculated from equation (29) is always larger than that calculated from equation (28). This implies that the Mangler's solution overpredicts the real value of the displacement thickness; that is, the transverse curvature acts to decrease the displacement thickness compared with Mangler's solution. This fact is also found in reference 2. Figure 3 shows that the value of δ^*/r_w increases as A increases; so A can be considered as a parameter for the effect of body transverse curvature. If A is not very small compared with unity the effect of transverse curvature needs to be taken into account. Figure 2 also shows that high wall temperatures yield larger κ's.

Contrary to the effect of A, increasing F_w will decrease the values of δ^*/r_w and κ (figs. 4 and 5). Figures 3 and 5 also indicate that a hot wall produces a larger displacement thickness because of the higher viscosity near the wall. The effects of A and F_w are smaller for cold walls.

The velocity (F') profiles and the effects of A and F_w on $F''(0)$ are given in figures 6 to 7. The value of $F''(0)$, which characterizes wall skin friction, increases with F_w and A. However, unlike the effect of F_w on F', F' approaches unity more slowly when A is large than when A is small. Generally, a higher wall temperature yields a larger $F''(0)$ for any given A. However, $F''(0)$ is not sensitive to the wall temperature variations for a given F_w. Only at very small F_w, hot walls can result in slightly higher $F''(0)$ than are obtained for cold walls.

The value of $G'(0)$ characterizes the rate of heat transfer at the walls. For $A = 0$ and $F_w = 0$, figures 8 and 9 show that the adiabatic total wall enthalpy ratio G_{wr} is equal to 0.84 which is approximately equal to $\sqrt{Pr}$ in the present study. It is noted that G_{wr} increases with F_w and decreases with A. This implies that the enthalpy recovery factor $\tilde{r}$ defined by

$$h_r = h_e + \tilde{r}\,\frac{U_e^2}{2} \tag{30}$$

is affected not only by the Prandtl number but also by the streamwise pressure gradient dP_e/dX. The wall-temperature gradient $G'(0)$ has positive and negative values for $G_w < G_{wr}$ and $G_w > G_{wr}$, respectively. The absolute value of $G'(0)$ increases with A and F_w.

The total enthalpy profiles for various values of A and F_w for cold and hot walls are similar to the velocity profiles. However, the value of G monotonically increases or decreases to approach unity at the edge boundary for cold walls or hot walls, respectively. For $G_w = 1.0$, which is close to

the value for the insulated wall, the total enthalpy profile shows some interesting properties. In figure 10, it is seen that the value of G decreases first to reach a minimum and then increases to a maximum exceeding unity, and then decreases to unity with increasing η. It indicates that the total enthalpy of the boundary-layer flow can exceed that in the outer inviscid flow for some ranges. The minimum and maximum values of G in the profile are larger and occur at lower heights for larger values of F_w. Conversely, the minimum and maximum values in the G profile are smaller and occur at higher heights when A is larger (fig. 11). This result agrees with the calculations in reference 2.

It is shown in figures 12 to 15 that wall cooling (low G_w) and mass bleeding (high F_w) tend to thin down the boundary-layer thickness and then decrease the strong interaction effects. The effect of F_w on P/P_∞ is smaller for cold walls. It is interesting that the transverse curvature effect has only a weak effect on the boundary-layer thickness $M_\infty\delta^*/X$ and the induced pressure P/P_∞. Since the Mangler's solution overpredicts the value of δ^*/r_w, we can conclude from equation (18) that $M_\infty\delta^*/X$ and P/P_∞ are underpredicted by the Mangler's solutions. It is noted that, for a hypersonic viscous flow over a flat plate, Li (refs. 7 and 13) also demonstrated that the induced pressure P/P_∞ and displacement thickness $M_\infty\delta^*/X$ increase with increasing wall temperature.

Both the skin friction coefficient $C_{f\infty}$ and the Stanton number St_∞ are shown (figs. 16 to 19) to increase with A, F_w, and G_w. These results are also shown in references 7 and 13 for a flat plate calculation. In the present study, calculations show that $C_{f\infty}$ and St_∞ are insensitive to the variation of A and F_w for very cold walls. However, the results in reference 7 conclude that $C_{f\infty}$ and St_∞ are insensitive to the variation of F_w for the hot wall. This discrepancy may be due to the assumptions, $Pr = 1$, $\mu \propto T$, and $h_r/H_e = 1$, that were made in the calculations in reference 7. Experimental works are required for the confirmation of these theoretical studies.

CONCLUSION

The similar solution for a slender three-fourths-power body of revolution at hypersonic flight has been studied. Attention was paid to the effects of the wall temperature, mass bleeding, and transverse curvature in the strong pressure interaction region of the boundary layer. The compressible boundary-layer equations were transformed to a system of ordinary equations and then the Runge-Kutta technique with the modified Newton's method was applied to solve the resulting two-point boundary value problem.

Three parameters, G_w, A, and F_w, were defined to characterize the effects of wall temperature, transverse curvature, and mass bleeding, respectively. Analysis has shown that the Mangler's solution overpredicts the real value of displacement thickness δ^*/r_w and then underpredicts the induced pressure P/P_∞. The displacement thickness δ^*/r_w increases with increasing G_w and A, but decreases with increasing F_w. The velocity gradient F'', which characterizes the skin friction, was found to increase with G_w, A, and F_w. Solutions also showed that although $F''(0)$ is larger for larger A, the velocity ratio F' approaches unity more slowly when A is large than when it is small. Because of the pressure gradient, the insulated total wall enthalpy

ratio G_{wr} changes not only with Pr but also changes with A and F_w. The parameter G_{wr} increases with F_w and decreases slightly with A. The absolute value of the wall-temperature gradient G'(0) increases as the deviation of G_w from G_{wr} increases: G'(0) is positive when $G_w < G_{wr}$ and negative when $G_w > G_{wr}$. The G distribution for $G_w = 1$ shows that G decreases first to a minimum, then increases to a maximum exceeding unity, and then decreases to unity with increasing η. This means that the total enthalpy of the boundary-layer flow can exceed that in the outer inviscid flow for some ranges. The two extreme values in the G profile are larger and occur at lower heights for larger F_w. However, the influence of A produces the opposite effect in the G profile.

The similar solutions in the strong interaction region show that the mass bleeding parameter F_w can produce a significant increment in the induced pressure P/P_∞ and in the parameter $M_\infty\delta^*/X$; however, the transverse curvature parameter A has a weak effect on them. The skin friction coefficient C_f, the heat transfer parameter $G'(0)/[h_r/H_e - G(0)]$, and the Stanton number St all increase with increasing G_w, A, and F_w. Generally, a cold wall makes the flow insensitive to the variation of A and F_w.

Experimental data for the problem considered in the present study were not available to compare with our results. However, extensive experimental studies are definitely required to verify both qualitative and quantitative aspects of the theoretical predictions of the boundary-layer behavior.

APPENDIX

SYMBOLS

A	transverse curvature parameter
C_f	skin friction coefficient
C_p	specific heat at constant pressure
F_w	mass bleeding parameter
F'	velocity ratio
G	total enthalpy ratio
G_w	total wall enthalpy ratio
G_{wr}	adiabatic total wall enthalpy ratio
$G'(0)$	wall-temperature gradient
H	total enthalpy
h	enthalpy
h_r	recovery enthalpy (adiabatic wall enthalpy)
h_w	enthalpy at wall
k	coefficient of thermal conductivity
M	Mach number
N	ratio of the product of density and viscosity, $\rho\mu/\rho_w\mu_w$
Nu	Nusselt number
P	pressure
Pr	Prandtl number
R	square of radius ratio
Re	Reynold's number
$\tilde{R}$	gas constant
r	radius from the central axis
r_w	wall radius
$\tilde{r}$	enthalpy recovery factor
St	Stanton number

T temperature

U velocity component in X-direction

V velocity component in Y-direction

X,Y coordinate axes for the three-fourths-power body of revolution

α,β constants

$\bar{\alpha}_w$ surface inclination angle

γ specific heat ratio

δ^* displacement thickness

δ_M displacement thickness for Mangler's transformation

ε termination criterion

η transformed boundary layer

κ integral factor

κ_M value of κ for $A = 0$

μ coefficient of molecular viscosity

ξ transformed surface coordinate

Π constant

ρ density

χ pressure interaction parameter

ω constant

Subscripts:

e edge condition

M calculated by Mangler's transformation

m,n constants

r recovery (adiabatic wall) condition

w wall condition

wr wall value in adiabatic condition

X,Y coordinate axes for the three-fourths-power body of revolution

η derivative with respect to η

ξ derivative with respect to ξ

Superscripts:

ω constant

REFERENCES

1. Hayes, W.D.; and Probstein, R.F.: Hypersonic Flow Theory, Academic Press, 1959, p. 361.

2. Yasuhara, M.: Axisymmetric Viscous Flow Past Very Slender Bodies of Revolution. J. Aerospace Sci., vol. 29, no. 6, June 1962, pp. 667-679, 688.

3. Probstein, R.F.; and Elliot, D.: The Transverse Curvature Effect in Compressible Axially Symmetric Laminar Boundary-Layer Flow. J. Aeronaut. Sci., vol. 23, no. 3, Mar. 1956, pp. 208-224, 236.

4. Yasuhara, M.: On the Hypersonic Viscous Flow Past a Flat Plate With Suction or Injection. J. Phys. Soc. Jpn., vol. 12, no. 2, Feb. 1957, pp. 177-182.

5. Lew, H.G.; and Fanucci, J.B.: On the Laminar Compressible Boundary Layer Over a Flat Plate With Suction or Injection. J. Aeronaut. Sci., vol. 22, no. 9, Sept. 1955, pp. 589-597.

6. Tien, C.L.: On Hypersonic Viscous Flow Over an Insulated Flat Plate With Surface Mass Transfer. J. Aerospace Sci., vol. 29, no. 9, Sept. 1962, pp. 1024-1028.

7. Li, T.Y.; and Gross, J.F.: Hypersonic Strong Viscous Interaction on a Flat Place with Surface Mass Transfer. Proceedings of the 1961 Heat Transfer and Fluid Mechanics Institute, R.C. Binder, et al., eds., Stanford University Press, 1961, pp. 146-160.

8. White, F.M.: Viscous Fluid Flow, McGraw Hill, 1974, p. 725.

9. Nagamatsu, H.T.: Summary of Recent GALCIT Hypersonic Experimental Investigations. J. Aeronaut. Sci., vol. 22, no. 3, Mar. 1955, pp. 165-172.

10. Hammitt, A.G.; and Bogdonoff, S.M.: A Study of the Flow About Simple Bodies at Mach Numbers from 11 to 15. Princeton Univ., Dept. of Aeronautical Engineering, Rept. No. 277, Sept. 1954.

11. Lees, L.: Influence of the Leading-Edge Shock Wave on the Laminar Boundary Layer at Hypersonic Speeds. California Institute of Technology, Guggenheim Aeronautical Lab Report TR-1, July 1954.

12. Yasuhara, M.: On the Hypersonic Viscous Flow Past Slender Bodies of Revolution. J. Phys. Soc. Jpn., vol. 11, no. 8, Aug. 1956, pp. 878-886.

13. Li, T.Y., and Nagamatsu, H.T.: Hypersonic Viscous Flow on Noninsulated Flat Plate. Proceedings of the 4th Midwestern Conference on Fluid Mechanics, R.C. Binder, ed., Purdue Univ., Lafayette, IN, 1955, pp. 273-287.

BIBLIOGRAPHY

Cohen, C.B.; and Reshotko, E.: Similar Solutions for the Compressible Laminar Boundary Layer With Heat Transfer and Pressure Gradient. NACA TN-3325, 1955.

Hayes, W.D.: On Laminar Boundary Layers With Heat Transfer. Jet Propulsion, vol. 26, no. 4, Apr. 1956, pp. 270-274.

Lees, L.: On the Boundary-Layer Equations in Hypersonic Flow and Their Approximate Solutions. J. Aeronaut. Sci., vol. 20, no. 2, Feb. 1953, pp. 143-145.

Lees, L.; and Probstein, R.F.: Hypersonic Viscous Flow Over a Flat Plate. Princeton Univ., Dept. of Aerospace Engineering, Rept. No. 195, 1952.

Nagakura, T.; and Naruse, H.: An Approximate Solution of the Hypersonic Laminar Boundary-Layer Equations and Its Application. J. Phys. Soc. Jpn., vol. 12, no. 11, Nov. 1957, pp. 1298-1304.

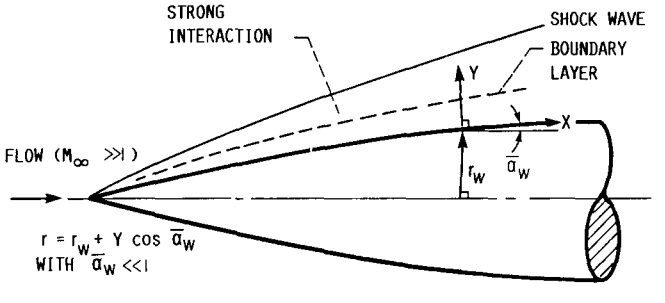

FIGURE 1. - COORDINATE SYSTEM FOR THE THREE-FOURTHS-POWER BODY OF REVOLUTION.

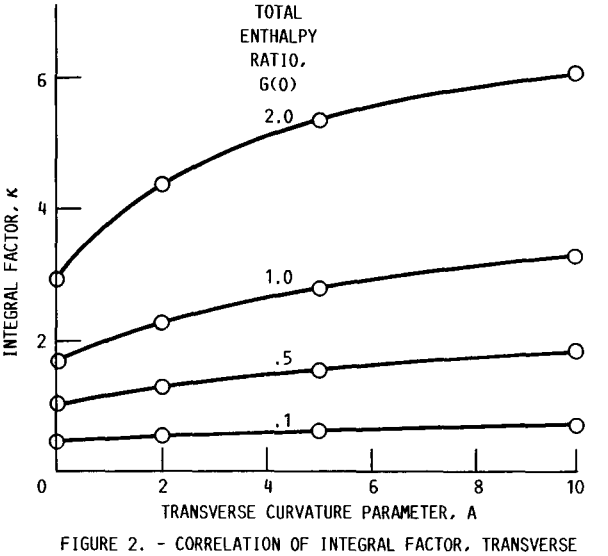

FIGURE 2. - CORRELATION OF INTEGRAL FACTOR, TRANSVERSE CURVATURE PARAMETER, AND TOTAL WALL ENTHALPY RATIO FOR A MASS BLEEDING PARAMETER OF 0.0.

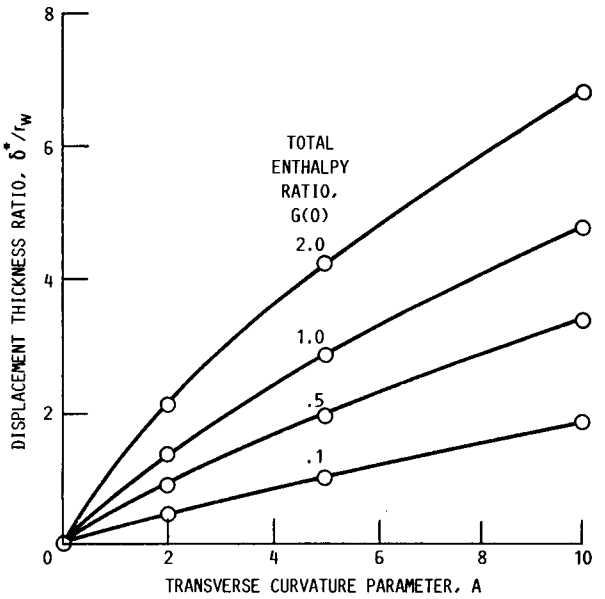

FIGURE 3. - CORRELATION OF DISPLACEMENT THICKNESS RATIO, TRANSVERSE CURVATURE PARAMETER, AND TOTAL WALL ENTHALP RATIO FOR A MASS BLEEDING PARAMETER OF 0.0.

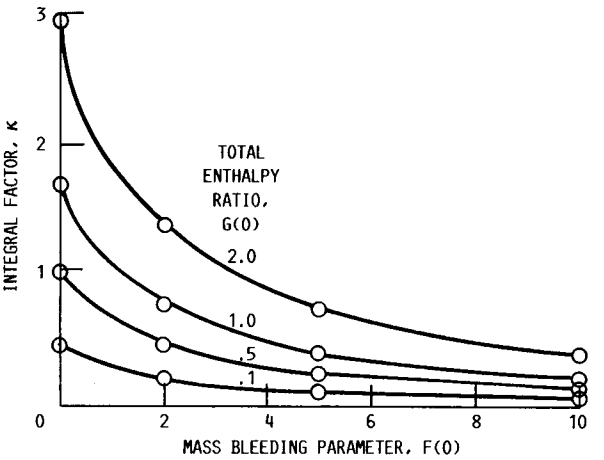

FIGURE 4. - CORRELATION OF INTEGRAL FACTOR, MASS BLEEDING PARAMETER, AND TOTAL WALL ENTHALPY RATIO FOR A TRANSVERSE CURVATURE PARAMETER OF 0.0.

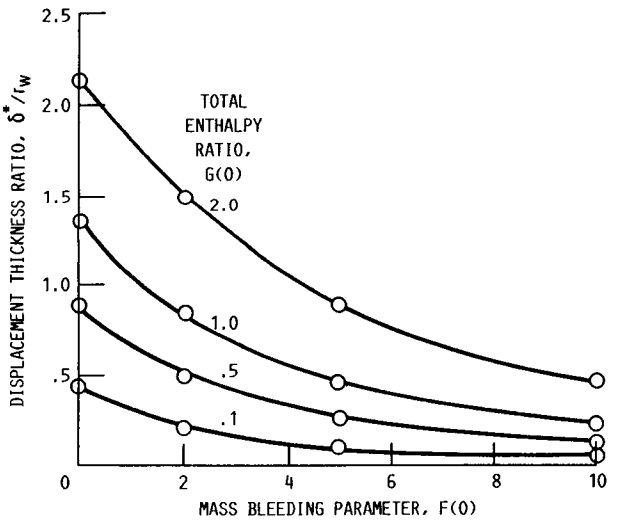

FIGURE 5. - CORRELATION OF DISPLACEMENT THICKNESS RATIO, MASS BLEEDING PARAMETER, AND TOTAL ENTHALPY RATIO FOR A TRANSVERSE CURVATURE PARAMETER OF 2.0.

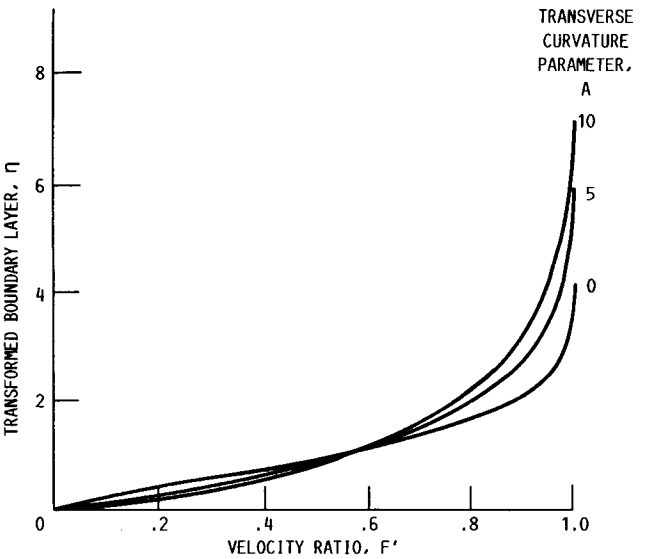

FIGURE 6. - CORRELATION OF TRANSFORMED BOUNDARY LAYER, VELOCITY RATIO ($F' = U/U_e$), AND TRANSVERSE CURVATURE PARAMETER FOR A TOTAL WALL ENTHALPY RATIO OF 0.1 AND A MASS BLEEDING PARAMETER OF 0.0.

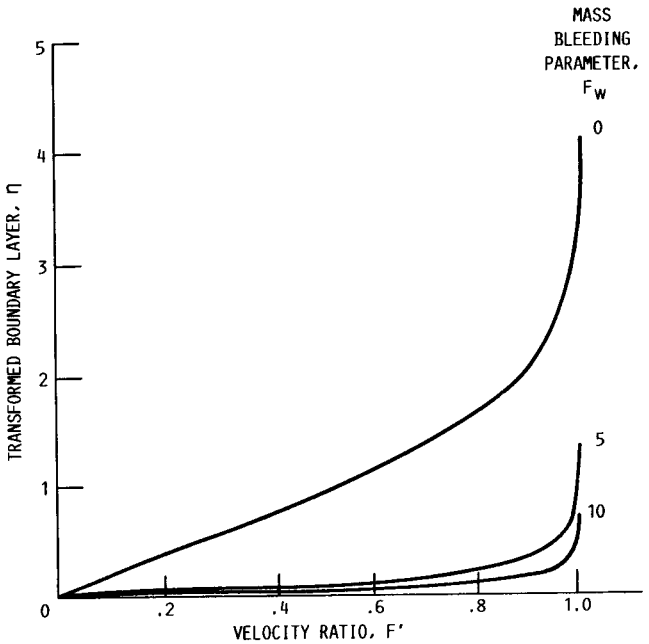

FIGURE 7. - CORRELATION OF TRANSFORMED BOUNDARY LAYER, VELOCITY RATIO ($F' = U/U_e$), AND MASS BLEEDING PARAMETER FOR A TOTAL WALL ENTHALPY RATIO OF 0.1 AND A TRANSVERSE CURVATURE PARAMETER OF 0.0.

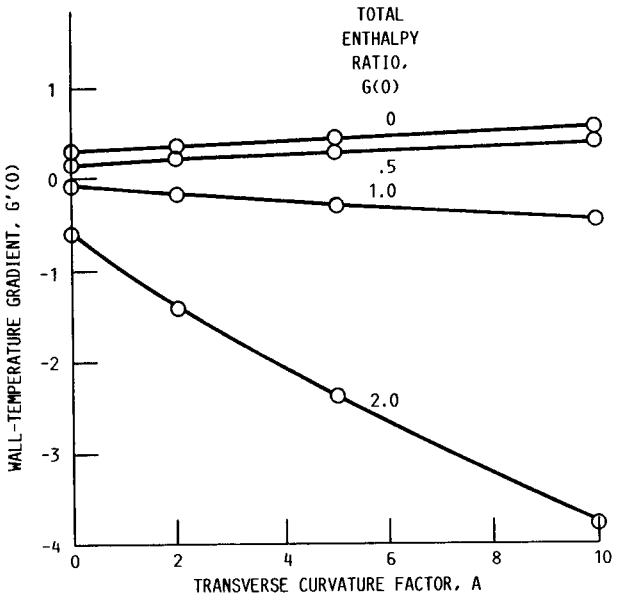

FIGURE 8. - CORRELATION OF WALL-TEMPERATURE GRADIENT, TRANSVERSE CURVATURE PARAMETER, AND TOTAL WALL ENTHALPY RATIO FOR A MASS BLEEDING PARAMETER OF 0.0.

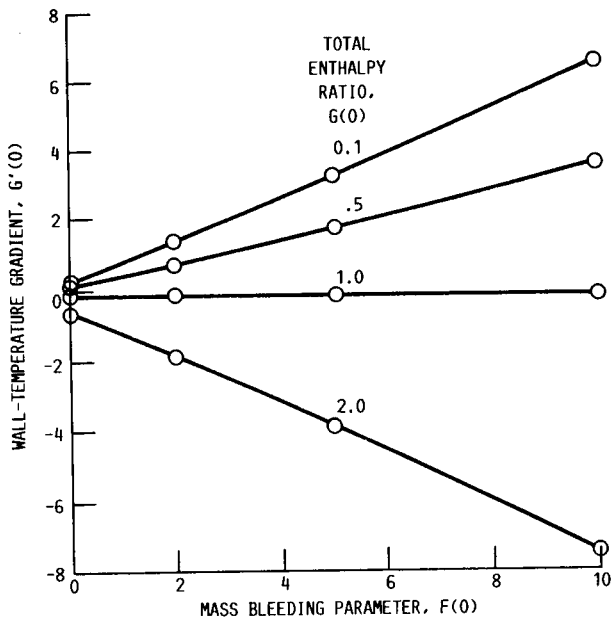

FIGURE 9. - CORRELATION OF WALL-TEMPERATURE GRADIENT, MASS BLEEDING PARAMETER, AND TOTAL WALL ENTHALPY RATIO FOR A TRANSVERSE CURVATURE PARAMETER OF 0.0.

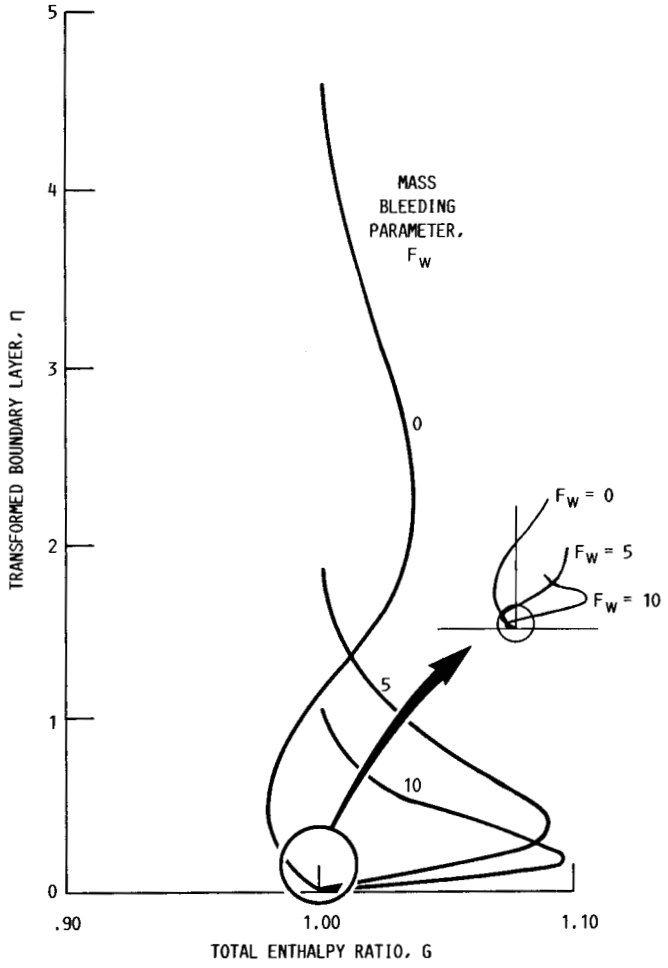

FIGURE 10. - CORRELATION OF TRANSFORMED BOUNDARY LAYER, TOTAL ENTHALPY RATIO ($G = H/H_e$), AND MASS BLEEDING PARAMETER FOR A TOTAL WALL ENTHALPY RATIO OF 1.0 AND A TRANSVERSE CURVATURE PARAMETER OF 0.0.

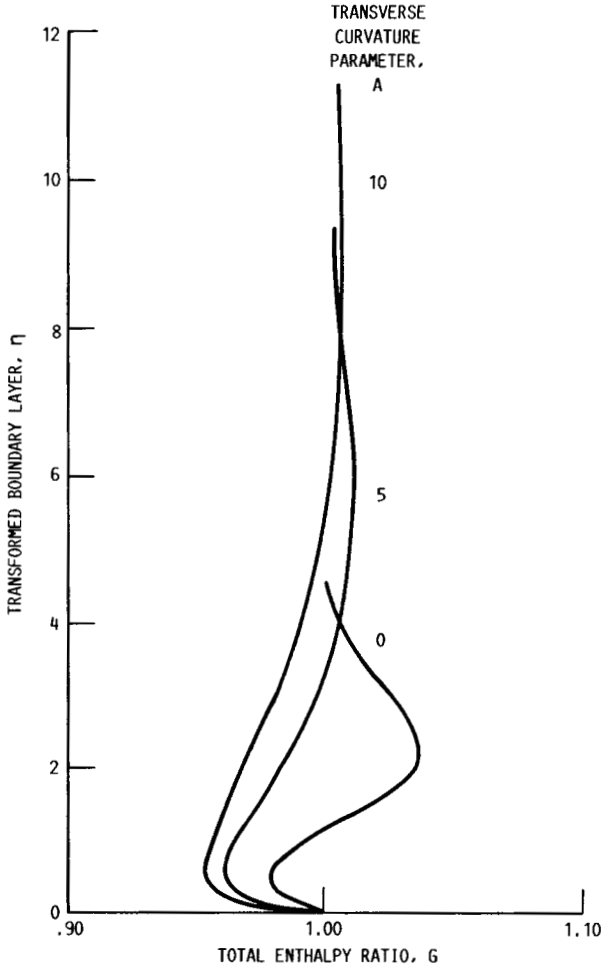

FIGURE 11. - CORRELATION OF TRANSFORMED BOUNDARY LAYER, TOTAL ENTHALPY RATIO ($G = H/H_e$), AND TRANSVERSE CURVATURE PARAMETER FOR A TOTAL WALL ENTHALPY RATIO OF 1.0 AND A MASS BLEEDING PARAMETER OF 0.0.

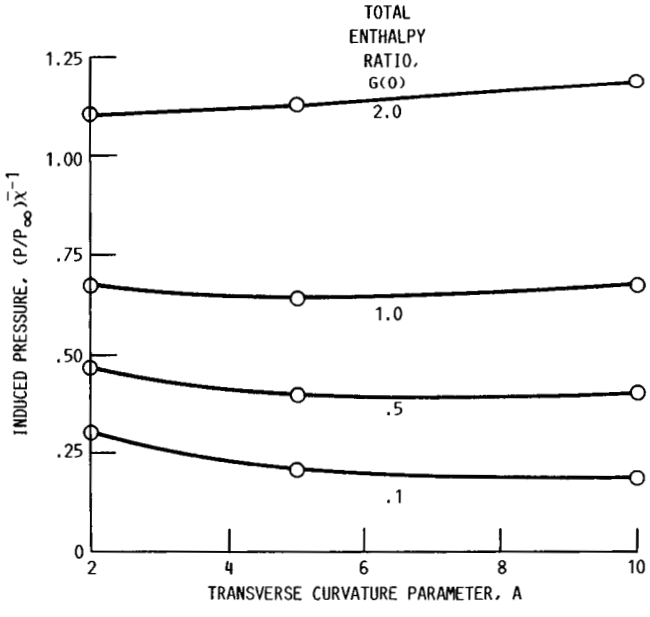

FIGURE 12. - CORRELATION OF INDUCED PRESSURE, TRANSVERSE CURVATURE PARAMETER, AND TOTAL WALL ENTHALPY RATIO FOR A MASS BLEEDING FACTOR OF 0.0.

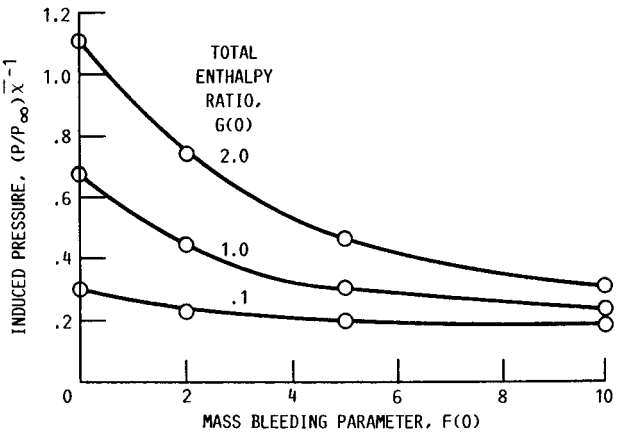

FIGURE 13. - CORRELATION OF INDUCED PRESSURE, MASS BLEEDING PARAMETER, AND TOTAL WALL ENTHALPY RATIO FOR A TRANSVERSE CURVATURE PARAMETER OF 2.0.

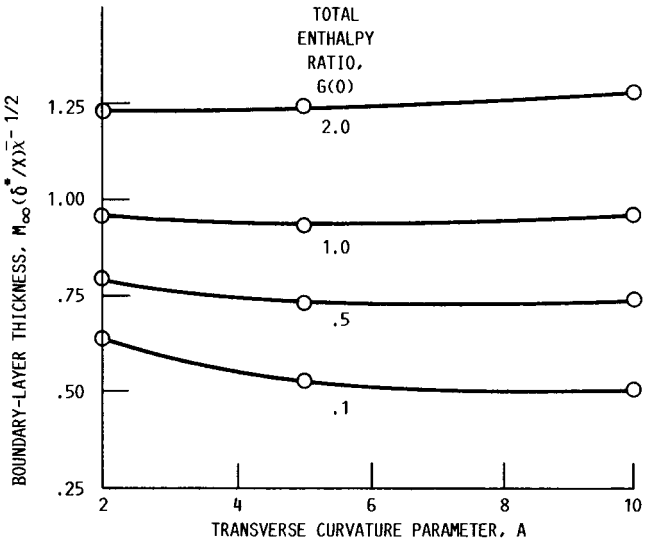

FIGURE 14. - CORRELATION OF BOUNDARY-LAYER THICKNESS, TRANSVERSE CURVATURE PARAMETER, AND TOTAL WALL ENTHALPY RATIO FOR A MASS BLEEDING PARAMETER OF 0.0.

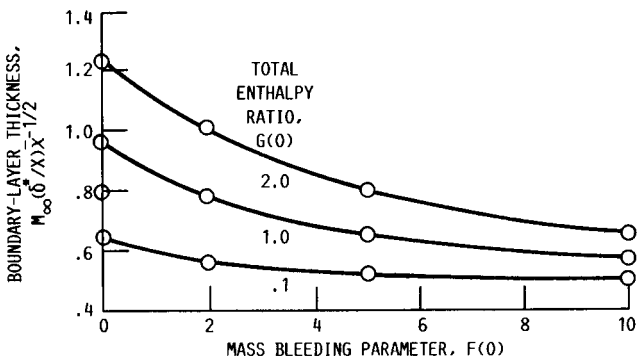

FIGURE 15. - CORRELATION OF BOUNDARY-LAYER THICKNESS, MASS BLEEDING PARAMETER, AND TOTAL WALL ENTHALPY RATIO FOR A TRANSVERSE CURVATURE PARAMETER OF 2.0.

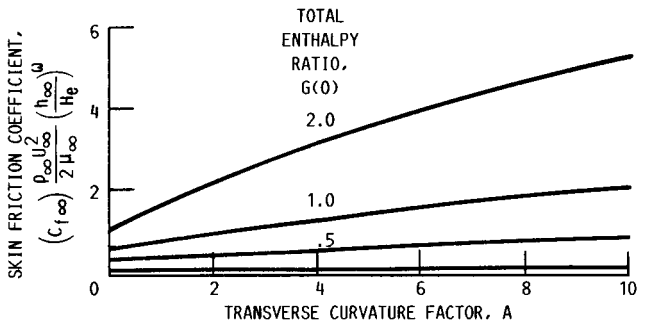

FIGURE 16. - CORRELATION OF SKIN FRICTION COEFFICIENT, TRANSVERSE CURVATURE PARAMETER, AND TOTAL WALL ENTHALPY RATIO FOR A MASS BLEEDING PARAMETER OF 0.0.

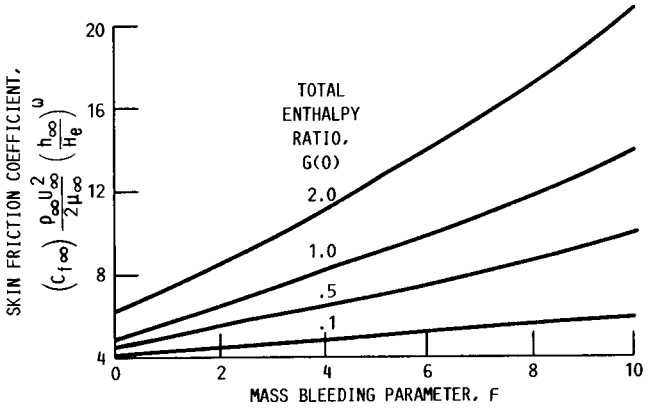

FIGURE 17. - CORRELATION OF SKIN FRICTION COEFFICIENT, MASS BLEEDING PARAMETER, AND TOTAL WALL ENTHALPY RATIO FOR A TRANSVERSE CURVATURE PARAMETER OF 2.0.

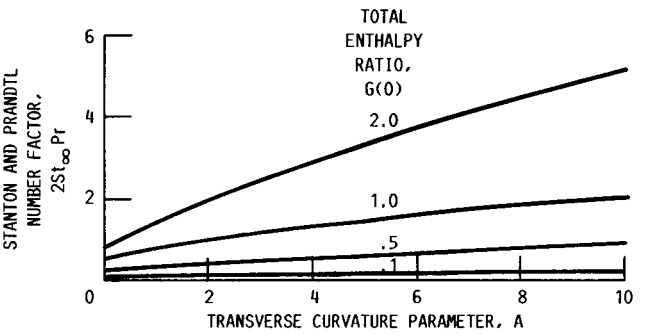

FIGURE 18. - CORRELATION OF STANTON AND PRANDTL NUMBER FACTOR, TRANSVERSE CURVATURE PARAMETER, AND TOTAL WALL ENTHALPY RATIO FOR A MASS BLEEDING PARAMETER OF 0.0.

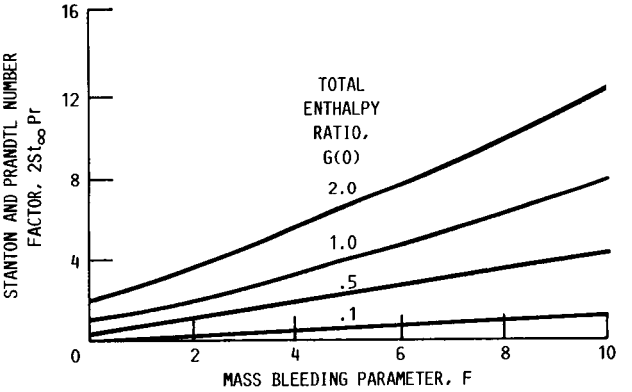

FIGURE 19. - CORRELATION OF STANTON AND PRANDTL NUMBER FACTOR, MASS BLEEDING PARAMETER, AND TOTAL WALL ENTHALPY RATIO FOR A TRANSVERSE CURVATURE PARAMETER OF 2.0.

NASA
National Aeronautics and Space Administration

Report Documentation Page

1. Report No.	2. Government Accession No.	3. Recipient's Catalog No.
NASA TM-100205 ICOMP-87-7		

4. Title and Subtitle	5. Report Date
Similar Solutions for Viscous Hypersonic Flow Over a Slender Three-Fourths-Power Body of Revolution	December 1987
	6. Performing Organization Code
7. Author(s)	8. Performing Organization Report No.
Chin-Shun Lin	E-3803
	10. Work Unit No.
	505-62-21
9. Performing Organization Name and Address	11. Contract or Grant No.
National Aeronautics and Space Administration Lewis Research Center Cleveland, Ohio 44135-3191	
	13. Type of Report and Period Covered
12. Sponsoring Agency Name and Address	Technical Memorandum
National Aeronautics and Space Administration Washington, D.C. 20546-0001	14. Sponsoring Agency Code

15. Supplementary Notes

Chin-Shun Lin, Institute for Computational Mechanics in Propulsion, NASA Lewis Research Center (work funded under Space Act Agreement C99066G).

16. Abstract

For hypersonic flow with a shock wave, there is a similar solution consistent throughout the viscous and inviscid layers along a very slender three-fourths-power body of revolution. The strong pressure interaction problem can then be treated by the method of similarity. In the present study, numerical calculations are performed in the viscous region with the edge pressure distribution known from the inviscid similar solutions. The compressible laminar boundary-layer equations are transformed into a system of ordinary differential equations. The resulting two-point boundary value problem is then solved by the Runge-Kutta method with a modified Newton's method for the corresponding boundary conditions. The effects of wall temperature, mass bleeding, and body transverse curvature are investigated. The induced pressure, displacement thickness, skin friction, and heat transfer due to the previously mentioned parameters are estimated and analyzed.

17. Key Words (Suggested by Author(s))	18. Distribution Statement
Similar solutions; Viscous hypersonic flow; Strong pressure interaction; Wall cooling; Mass bleeding; Body transverse curvature	Unclassified - Unlimited Subject Category 34

19. Security Classif. (of this report)	20. Security Classif. (of this page)	21. No of pages	22. Price*
Unclassified	Unclassified	22	A02

NASA FORM 1626 OCT 86

*For sale by the National Technical Information Service, Springfield, Virginia 22161